IEEE Access
Multidisciplinary | Rapid Review | Open Access Journal

Received May 14, 2019, accepted June 6, 2019, date of publication June 12, 2019, date of current version June 26, 2019.

Digital Object Identifier 10.1109/ACCESS.2019.2922358

Solar Array Fed Synchronous Reluctance Motor Driven Water Pump: An Improved Performance Under Partial Shading Conditions

MOHAMED N. IBRAHIM[1,2,3], HEGAZY REZK[4,5], MUJAHED AL-DHAIFALLAH[6], AND PETER SERGEANT[1,2], (Member, IEEE)

[1]Department of Electrical Energy, Metals, Mechanical Constructions and Systems, Ghent University, 9000 Ghent, Belgium
[2]Core Lab EEDT-MP, Flanders Make, 3001 Leuven, Belgium
[3]Electrical Engineering Department, Kafrelshiekh University, Kafr el-Sheikh 33511, Egypt
[4]College of Engineering at Wadi Addawaser, Prince Sattam Bin Abdulaziz University, Wadi Aldawaser 11991, Saudi Arabia
[5]Electrical Engineering Department, Faculty of Engineering, Minia University, Minia 61111, Egypt
[6]Systems Engineering Department, King Fahd University of Petroleum and Minerals, Dhahran 31261, Saudi Arabia

Corresponding author: Mujahed Al-Dhaifallah (mujahed@kfupm.edu.sa)

This work was supported by the Special Research Fund of Ghent University [Bijzonder Onderzoeksfonds (BOF)]: BOF 2014.

ABSTRACT An improved performance of a photovoltaic (PV) pumping system employing a synchronous reluctance motor (SynRM) under partial shading conditions is proposed. The system does not include the dc–dc converter that is predominantly being utilized for maximizing the output power of the PV array. In addition, storage batteries are also not contained. A conventional inverter connected directly to the PV array is used to drive the SynRM. Further, a control strategy is proposed to drive the inverter so that the maximum output power of the PV array is achieved while the SynRM is working at the maximum torque per Ampère condition. Consequently, this results in an improved system efficiency and cost. Moreover, two maximum power point tracking (MPPT) techniques are compared under uniform and partial shadow irradiation conditions. The first MPPT algorithm is based on the conventional perturbation and observation (P&O) method and the second one uses a differential evolution (DE) optimization technique. It is found that the DE optimization method leads to a higher PV output power than using the P&O method under the partial shadow condition. Hence, the pump flow rate is much higher. However, under a uniform irradiation level, the PV system provides the available maximum power using both MPPT techniques. The experimental measurements are obtained to validate the theoretical work.

INDEX TERMS Photovoltaic pumping system, maximum power point trackers, synchronous reluctance machines, motor drives.

I. INTRODUCTION

In the recent days, solar photovoltaic (PV) systems have been played a key role in the renewable energy systems, due to the availability of the solar irradiance in contrast to the other renewable energy sources (RESs). They have many advantages such as free access to them, inexhaustibility, cleanness and low maintenance [1]–[4]. Further, thanks to the progress in the production technology of the PV cells, their price is decreasing dramatically [1].

The solar system could work as a standalone (off grid) or connected to the grid. The standalone PV systems are employed in several developing countries e.g. Egypt, Sudan, Algeria, India etc. [2], [5]–[8], particularly in the remote areas from the grid [1], [4]. Several developing countries, in particular African countries, have a quite availability of the sun. For instance, Egypt has an average sun irradiation level of about 600 W/m^2 [9], [10]. This encourages to install standalone PV systems for pumping applications. A detailed analysis about the investigation on a site-specific application of solar PV pumping systems in different countries are given in [2]. The main conclusion from [2] is that the solar system is an effective, sustainable and easy way to pump the water for irrigations and house needs. Nevertheless, the price of the solar PV modules and the efficiency of the whole system are still great challenges. Accordingly, various literature research is being carried out to improve the whole efficiency of the solar pumping system as well as to minimize the cost.

The associate editor coordinating the review of this manuscript and approving it for publication was B. Chitti Babu.

Several authors have addressed the selection of the electric motor that is employed in PV pumping system [2]–[4], [9]–[18]. In the past, the solar pumping system used mainly the brushed DC motors. The main advantage of this system is that the DC motors can be simply directly connected to the solar array. However, in this case the system performance might be not optimal. Hence, a DC-DC converter could be used to drive the system in an efficient way [11], [19]–[24]. The transient and steady state performances of direct coupling of several types of DC motors to a PV supplied water pumping system were investigated in [19]–[24]. These papers showed the influence of different irradiation levels, loading conditions and several controllers on the PV system. It was found that the separately excited and PMDC motors are more appropriate than both the shunt and series DC machines for PV water pumping systems [22]–[26]. Nevertheless, DC motors experience several disadvantages due to the brush contacts and commutator. This requires frequent maintenances and increases running cost that reduces the reliability and efficiency of the system [25]–[27]. Consequently, the brushless machines are receiving a great attention in the pumping systems because of their merits, particularly the low running cost and the high efficiency [4].

Considerable literature publications have been investigated the solar pumping systems when brushless DC motors (BDCMs), induction motors (IMs), PM synchronous motors (PMSMs) and switched reluctance motors (SRMs) are employed [12], [13], [14], [15], [27]. The solar pumping systems using BDCMs have been extremely investigated in the literature. This is because they have several advantages such as high robustness and efficiency. A single stage PV array fed BDCM driven water pump is presented in [28]. This system does not use the conventional DC-DC converter. However, there is a need for three hall sensors to accomplish the electronic commutation to drive the system at the maximum power point of the PV array. The IMs are utilized in solar systems in [29] and [30] for water pumping based on an inverter without using a DC-DC converter. However, as known, the IMs experience a relatively lower efficiency, in particular under partial loading cases due to the domination of the copper losses [17]. Consequently, these disadvantages motivate using the PMSMs. In [14], a PMSM fed from a solar array and driven a water pump, as an example of a standalone solar system, is studied. However, this study does not take into account the inverter losses. In addition, the PMs suffer from the unstable market in terms of the availability and the prices. Furthermore, the demagnetization due to the weather conditions – in particular in the harsh environments where the ambient temperature might be high– is a great challenge. Hence, reluctance machines have been considered as good candidates in the pumping systems [30]–[33].

For pumping systems in developing countries, synchronous reluctance motors (SynRMs) offer many merits in contrast to the various kinds of electric motors. These merits include a simple structure and a low cost. Besides, they do not have windings, cage and magnets in the rotor, hence they have a better temperature distribution. Furthermore, they have acceptable efficiency, which is better than that of IM and behind that PMSM [31]. However, limited research work was done regarding the PV pumping systems using SynRMs [3], [4], [32]. The design considerations of a solar pumping system using SynRM is shown in [3]. In addition, [4] presented a control method to enhance the performance of the solar system shown in [3]. However, both [3] and [4] considered a SynRM of axially laminated caged rotor. This rotor type leads to an increased losses and it is difficult to be manufactured. Besides, an approximated model of the SynRM was used in which the core saturation impact on the inductance of the machine was neglected. This results in a deviation in the predicted SynRM output power, hence the whole performance of the system [18]. Further, the geometry of the SynRM and the PV modules arrangement were not optimally designed. Furthermore, maximizing the output power of the PV array is done using a boost converter which makes the system more costly and complex. Recently, the authors of [32] presented an analysis and design of a PV pumping system using a SynRM. However, the PV pumping system includes DC-DC boost converter to maximize the PV output power. Moreover, [33] has presented an investigation of PV pumping system utilizing a SynRM, without using batteries. The conventional inverter is employed to drive the motor and to maximize the PV output power of the array. However, a uniform solar irradiation distribution over all the PV modules is assumed i.e. no partial shadow on the PV modules is occurred. In addition, a conventional maximum power point tracking method (MPPT), i.e. perturbation and observation (P and O) method, is used to maximize the PV output power.

To this end, the presented manuscript extends the work in [33] and aims to further investigate the influence of partial shadow condition on the performance of the PV system employing SynRM. Compared to the conventional P and O MPPT method, an optimization technique is proposed to further improve the whole system performance. In this paper, section II provides the design of the various components of the whole system; section III investigates the control of the proposed system; the performance of the whole system using two different MPPT techniques under uniform and shadow conditions is presented in section IV; experimental validation is shown in section V. Finally, conclusions of this work are highlighted in section VI.

II. DESIGN OF THE PROPOSED PV PUMPING SYSTEM

The schematic diagram of the proposed PV pumping system is sketched in Fig. 1. The system consists of the following components:

- PV array;
- Conventional voltage source inverter (VSI);
- Three phase synchronous reluctance motor (SynRM);
- Centrifugal pump;
- Control system

The proposed PV pumping system is employed for pumping water for the purposes of irrigation and human needs in

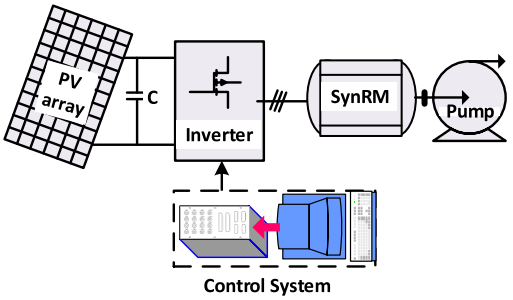

FIGURE 1. Schematic diagram of the proposed PV pumping system.

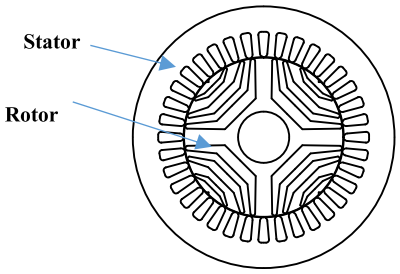

FIGURE 2. Schematic diagram of the SynRM geometry.

the rural regions in which the connection to the grid is not possible or costly. It is well-known that the required amount of water depends on the area of the agriculture land and the number of persons. It is assumed that the mean required amount of water is about 350 m^3/day. To achieve this amount of water (350 m^3/day), it is necessary to know approximately the available period in which the motor drives the pump. This depends on various factors e.g. weather, season, country etc. Hence, the number of sunny hours is assumed to be 10 hours/day. Consequently, the mean pump flow rate is 35 m^3/hour. The height difference (the head) of the water is 35 m as an assumption. Hence, the required mean output power of the pump can be computed based on the flow rate and the height difference as will be shown later.

A. DESIGN OF THE CENTRIFUGAL PUMP

Using the flow rate and the total head, the output power of the pump is expressed as follows [34], [35]:

$$P_p = \frac{\rho g}{3600} QH \tag{1}$$

where ρ is the water density (kg/m^3); g is the gravitational constant (9.81 m/s^2); Q is the flow rate (m^3/h); H is the total head (m) of the pump.

According to the aforementioned flow rate (Q) and the total head (H) of the pump (35 m^3/hour, 35 m), the output power of the pump can be determined that equals to 3.33 kW. Hence, the input power of the pump can be calculated; it is 4.16 kW at an assumed pump efficiency of 80%.

B. DESIGN OF THE SYNCHRONOUS RELUCTANCE MOTOR (SynRM)

The rating of the SynRM is selected based on the characteristics of the pump (input mechanical power and speed). In addition, it is evident that the output power of the PV modules varies with both the sun irradiance and temperature levels. This means that the motor output power varies as well. Hence, the motor will not operate at the rated power during the whole operation period. Consequently, the motor rating is chosen to be a 5.5 kW so that the required amount of water can be achieved. Notice that, a margin factor is also considered in this power rating to cover the problem of lower irradiation levels. The SynRM geometry is sketched in Fig. 2 and its geometrical parameters are shown in Table 1. The initial motor geometry is selected based on the induction motor of similar rated power. The rotor geometry is optimized using finite element method (FEM) [18].

TABLE 1. SynRM specifications.

Variable	Value	Variable	Value
Stator slots/ poles	36/4	Stack length	140 mm
Flux barriers /pole	3	Rotor /stator steel	M330-50A/ M270-50A
Number of phases	3	Length of air gap	0.3 mm
Outer /inner diameter of the stator	180 mm/ 110 mm	Rated voltage/ current	380 V/12.23 A
Shaft diameter	35 mm	Rated power	5.5 kW
Outer diameter of the rotor	109.4 mm	Rated speed	3000 rpm

In order to control the motor in an efficient way in the PV pumping system, it is essential firstly to examine its performance. The SynRM performance is simulated using FEM. In the simulation, the current controlled inverter that supplies the SynRM is emulated by injecting a pure sinusoidal currents in the stator windings. In addition, the rotor speed is constant at the given value. This analysis neglects the harmonics in the injected currents of the stator coils. Eventually, the output power, power factor, torque ripple and efficiency can be obtained.

Figure 3 shows the output power of the SynRM as a function of the current angle for several stator currents at the

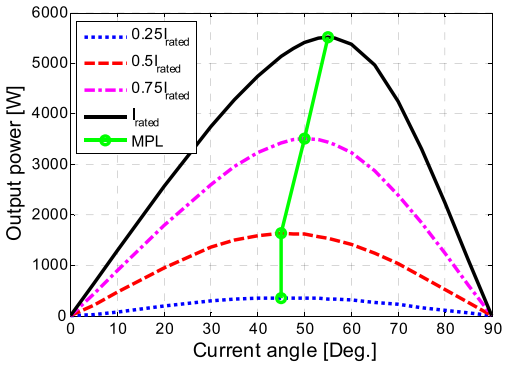

FIGURE 3. SynRM output power versus current angle at various stator current amplitudes and at the rated speed.

rated speed. The angle of the stator current vector with respect to the d-axis, as shown in [18], is defined as the current angle. For a fixed stator current amplitude, the variation of the current components (d and q axis) with the current angle results in a different SynRM output power. Besides, it is evident from Fig. 3 that the current angle of the maximum output power of the SynRM (MPL in Fig. 3) is not a fixed value but it depends on the current level because of the core saturation behavior of the machine. This can be noticed when comparing the current angle at 25% and 100% of the rated current: it is 45° at 25% of the rated current compared to 55° at the rated current. The green line shown in Fig. 3 indicates the maximum power locus (MPL) of the SynRM at various current amplitudes i.e. maximum power per Ampère.

Figure 4 displays the power factor of the motor versus the current angle and various stator current amplitudes and at the rated speed. It is obvious that the power factor of the motor increases when the stator current amplitude increases; it is also increases when the current angle increases up to a specific value and then it deceases. This means that there is an optimal current angle at which the SynRM is working at a maximum power factor. However, the optimal current angle of the maximum power factor is not constant, and it depends on the stator current level, similar trend as the output power (Fig. 3). The maximum power factor locus (MPFL) is shown in Fig. 4 (a cyan line). Figure 5 presents the torque ripple of the SynRM as a function of the current angle for various stator current amplitudes at the rated speed. For low and high current angles, the motor produces a high torque ripple. This is because the SynRM torque ripple is inversely proportional to the average torque, which is rather low for low and high current angles (see Fig. 3).

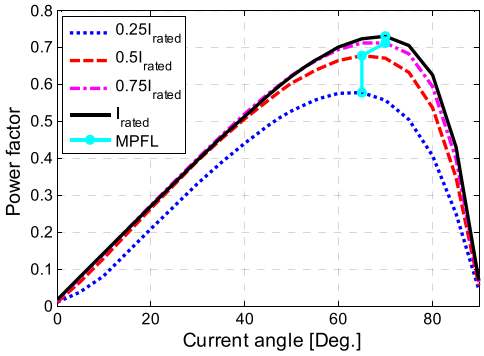

FIGURE 4. SynRM power factor versus current angle at various stator current amplitudes and at the rated speed.

From Figs. 3, 4 and 5, it is evident that at a given current amplitude the SynRM can be controlled to deliver the maximum available power, to work at the maximum power factor or to produce low torque ripple depending on the application. These features can be obtained by controlling the dq-axis current components of the motor via the current angle value.

The total losses and the simulated efficiency of the SynRM as functions of the current angle at the rated current and speed are reported in Figs. 6 and 7 respectively.

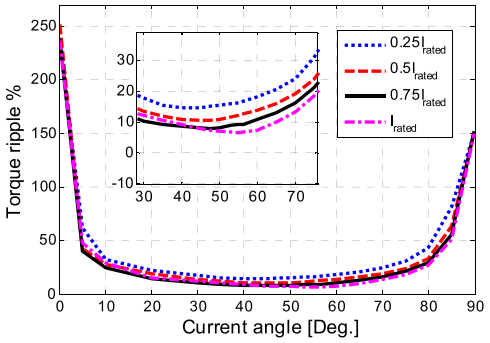

FIGURE 5. SynRM torque ripple % versus current angle at various stator current amplitudes and at the rated speed.

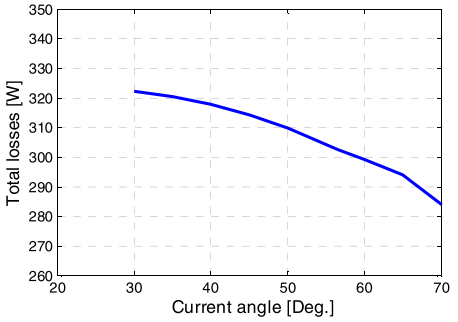

FIGURE 6. SynRM total losses versus current angle at various stator current amplitudes and at the rated speed.

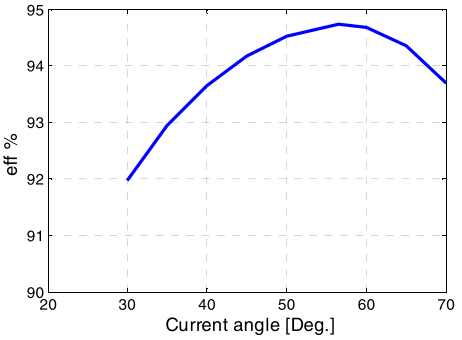

FIGURE 7. SynRM efficiency % versus current angle at various stator current amplitudes and at the rated speed.

The efficiency is computed using the output power and the total machine losses (core and copper losses). Notice that, the losses of the mechanical part and pulse width modulation of the currents are not taken into account. To compute the iron core losses, the flux density magnitude B is obtained from FEM solution of the SynRM. Thereafter, the iron core losses are determined using the method mentioned in [5]. The copper losses are calculated simply using the resistance and the current of the SynRM. It is observed that the SynRM losses, shown in Fig. 6, decreases when the current angle increases. This is because the flux density amplitude decreases, resulting in a decrease in the iron losses. Notice that the copper losses are constant for the same current amplitude. From Fig. 7, the SynRM efficiency is about 94.74% at the rated

current and speed and at the optimal current angle (maximum torque per Ampère). Moreover, the simulated efficiency map of the SynRM at the optimal current angles for currents and speeds up to the rated value is reported in Fig. 8. It is observed that the SynRM efficiency is about 84% for low speed and torque: which is rather high for such motor rating compared to the induction machines.

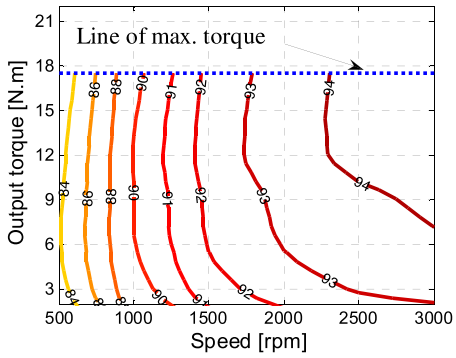

FIGURE 8. Simulated efficiency map (in percent) of the SynRM at the optimal current angles up to the rated current and speed.

C. DESIGN OF THE THREE PHASE VOLTAGE SOURCE INVERTER (VSI)

A conventional VSI is used in the proposed system. Figure 9 displays a sketch of the VSI that includes three legs of 2 IGBTs each.

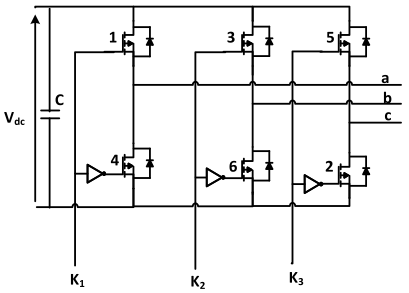

FIGURE 9. Schematic diagram of the VSI.

The rated power and power factor of the SynRM are used to calculate the rating of the inverter (kVA). A 10 kVA inverter is selected based on the output power (5.5 kW), efficiency (94.74%) and power factor (0.66) of the SynRM. In addition, an increase of a 10% is also taken into account in the inverter rating (10 kVA) as a margin factor. The DC link voltage of the inverter is 800 V to achieve the required motor rated voltage, considering a margin factor. The efficiency of the inverter is assumed to be 96%. The DC link capacitor is selected to be 1000 μF [1].

D. DESIGN OF THE PV ARRAY

The PV module mentioned in Table 2 is employed to construct the PV array. The voltage-power and voltage-current curves of the PV module at different solar irradiation levels and temperatures are shown in Figs. 10 and 11 respectively. Evidently, the irradiation level affects the output power of the solar PV module much more than the temperature.

TABLE 2. PV module specifications.

Variable	Symbol	Value
Maximum output power	P_{max}	135 W
Open circuit voltage	V_{oc}	22.1 V
Short circuit current	I_{sc}	8.37 A
Temperature coefficient (short circuit current)	k_i	$5.02e^{-3}$ A/°C
Temperature coefficient (open circuit voltage)	k_v	$-8e^{-2}$ V/°C
Reference temperature	T_{ref}	25°C

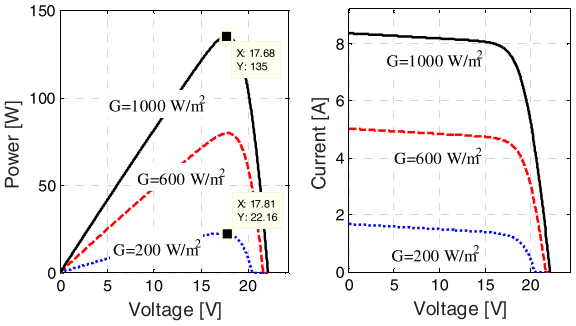

FIGURE 10. PV module characteristics at three solar irradiance levels (G = 200 W/m^2, 400 W/m^2 and 1000 W/m^2) and one temperature (T = 25°C).

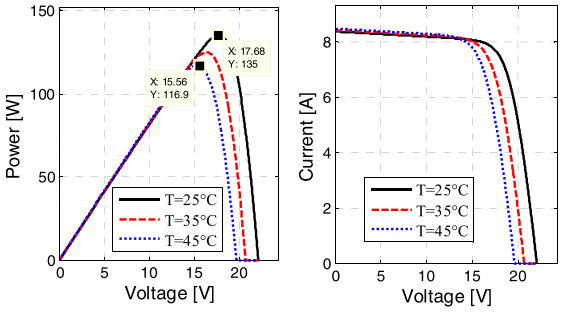

FIGURE 11. PV module characteristics at three temperatures (T = 25°C, 35°C and 45°C) and one solar irradiance level (G = 1000 w/m^2).

Based on the previous analysis (a, b and c), the required output power of the PV array is selected to be 5.66 kW. Consequently, the required number of PV modules is 42 of 135 W each (see Table 2). All the modules are connected in series in order to provide the necessary DC bus voltage and the motor current. The characteristics of the PV array are shown in Fig. 12 for various solar irradiance levels at T = 25°C, assuming a uniform distribution for the irradiation over all the PV modules. The green marker line in Fig. 12 indicates the maximum power line (a) and the corresponding voltage and current (b). Figure 13 shows the PV array characteristics under three different partial shadow patterns at T = 25°C. The total number of modules (42) is divided into two parts in Pattern 1 with two irradiation levels (G = 1000 W/m^2

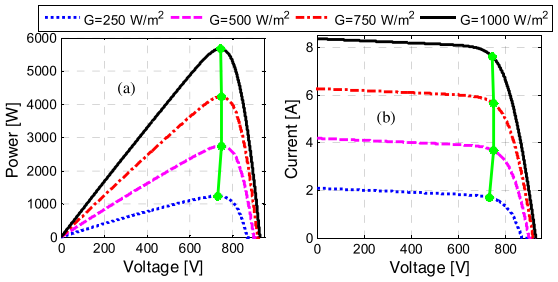

FIGURE 12. The PV array characteristics at various solar irradiance levels (G = 250 W/m^2, 500 W/m^2, 750 W/m^2 and 1000 W/m^2) with assuming a uniform irradiance distribution over all the modules and T = 25°C.

and 300 W/m^2), three parts in Pattern 2 with three irradiation levels (G = 1000 W/m^2, G = 800 W/m^2 and 400 W/m^2) and four parts in Pattern 3 with four irradiation levels (G = 1000 W/m^2, 800 W/m^2, 600 W/m^2 and 300 W/m^2). It is clear from Fig. 13 that the PV array output power under shadow condition has a global maximum power point.

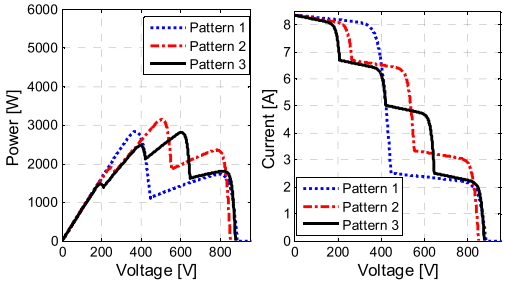

FIGURE 13. The PV array characteristics under three different shadow patterns (Pattern 1: G = 1000 W/m^2 and 300 W/m^2, Pattern 2: G = 1000 W/m^2, G = 800 W/m^2 and 400 W/m^2, and Pattern 3: G = 1000 W/m^2, 800 W/m^2, 600 W/m^2 and 300 W/m^2) and T = 25°C.

It is observed from Fig. 1 that the proposed system has neither DC-DC converter that is always used to maximize the output power of the PV array nor storage batteries. This is to reduce the losses and the cost of the system. Notice that, in some industrial application, a regulated DC- bus voltage and/or a battery storage is necessary. However, in case of the pumping system, both DC-DC converter and batteries could be removed [25]–[28].

III. THE CONTROL SYSTEM

The sketched of the whole system components is reported in Fig. 14. It is well-known that the SynRM is not a self-starting machine. This means that a control system is always necessary to drive the motor to work properly. In addition, the operating point of the PV array must be near maximum power point (MPP) to maximize the output power of PV system. Therefore, MPP tracking (MPPT) system is highly required. Use of MPPT leads certainly to increase PV system efficiency, accordingly reduces the total number of required PV modules, and therefore minimizes the capital system cost [36]. The control system of the proposed PV system includes two main parts: (a) the first part is based on the conventional field oriented control to drive the SynRM to maintain the maximum torque per Ampère condition, and (b) the second part is using a maximum power point strategy for maximizing the output of the PV array.

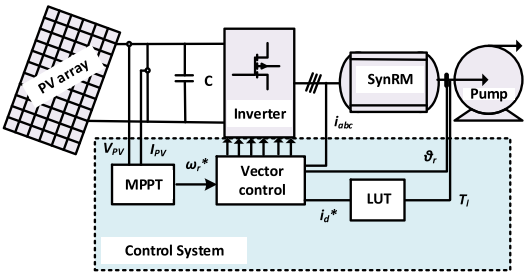

FIGURE 14. Sketch of the complete system.

A. FIELD ORIENTED CONTROL (FOC) TECHNIQUE

The conventional field oriented control (FOC) technique is employed to drive the SynRM. The diagram of FOC is shown in Fig. 15 in which two reference signals are required.

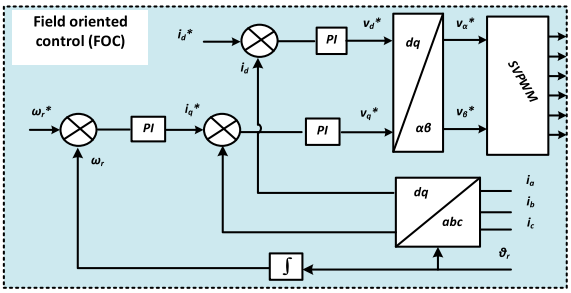

FIGURE 15. The diagram of the FOC.

The first set point signal is the speed (ω_r*) that is an effective factor in the PV pumping system; because the pump load torque is a function of the motor speed. The second set point of the FOC is the d-axis current (i_d*) which is responsible for driving the SynRM at the maximum torque per Ampère (the marker green line in Fig. 3). The set point of the current (i_d*) is obtained using the pump load torque from the lookup table (LUT), which is built from FEM. Three proportional integral (PI) controllers are employed: one PI controller for the speed loop and the remainder two PI controllers are used in the d and q axis current components loops. The parameters of the PI controllers can be obtained by several ways. A trial and error method is used to obtain the PI controller parameters in the simulation. However, an experimental method is implemented to obtain the parameters of the controllers in the experimental measurements. Moreover, a MPPT is necessary for maximizing the output power of the array. To drive the system efficiently, the locus of the maximum power of the PV array (i.e. the green marker line in Fig. 12) and the maximum power per Ampère of the SynRM have to be matched (the green marker line in Fig. 3). This can be done as follows. 1) The set point of the motor speed is obtained from the maximum power point tracker; 2) the set point of the d-axis current is obtained from the

lookup tables that is constructed from FEM simulations, in a similar manner as Fig. 37 (appendix section) [5].

B. MAXIMUM POWER POINT TRACKERS

The solar system contains several PV panels that are interconnected in series and/or in parallel to fulfill the desired system rating. Consequently, the conditions of partial shadow (CPS) can easily occurs. It takes place when a part of the PV array collects a non-uniform solar radiation [37]. The PV system should be built in a region free from shadow. It is commonly built in urban regions; thereby PV system can exposed to CPS e.g. caused by adjacent buildings. Consequently, the power-voltage curve of PV array has some local maximum points and one global point. This problem decreases the efficiency of conventional MPP tracking techniques [38], [39]. The conventional MPPTs were proposed to increase PV system efficiency under normal conditions [40]. Such techniques comprise as an example: hill climbing and P&O method. Although, the conventional MPPTs are successfully extract MPP under uniform irradiance, where only a unique MPP appears at power-voltage curve. In contrast, such MPPTs cannot deal very efficient under CPS, where the PV characteristics include several MPPs [42]. Consequently, PV system efficiency is reduced. To solve this dilemma, employing meta-heuristic optimizers for extracting global MPP has been initiated [36]–[53]. Such algorithms include for instance Flower Pollination [42], Differential Evolution [41], Cuckoo Search [37], Shuffled Frog Leap Algorithm [43], Particle Swarm Optimization [38], Ant Colony Optimization [44], Teaching–Learning-Based Optimization [49] and Mine Blast Optimization [50]. Two maximum power point tracking techniques are compared in this study: (a) conventional perturbation and observation (P&O) method and (b) differential evaluation (DE) based global technique.

1) CONVENTIONAL PERTURBATION AND OBSERVATION (P&O) MPPT TECHNIQUE

The flow chart of the conventional P&O MPPT strategy is shown in Fig. 16. In this technique, first, the PV array voltage and current are measured. Then, the output power of the array is computed. The present value at time instant m of the measured PV power and voltage are compared with the previous values at time instant m-1; the time difference between the two instants is one sample time (1e-5 s). At the end, the reference speed of the motor is obtained as shown in Fig. 16. This speed ensures maximizing the output power of the PV array.

2) DIFFERENTIAL EVOLUTION (DE) BASED GLOBAL MPPT TECHNIQUE

The DE based global MPPT technique is considered one of the most popular optimizers that is employed to tackle global optimization problems. It starts the solution process with random population. Next, the mutation, crossover, and selection stages are taken place to modify the population throughout the evolution in the direction of the optimal solution. More details

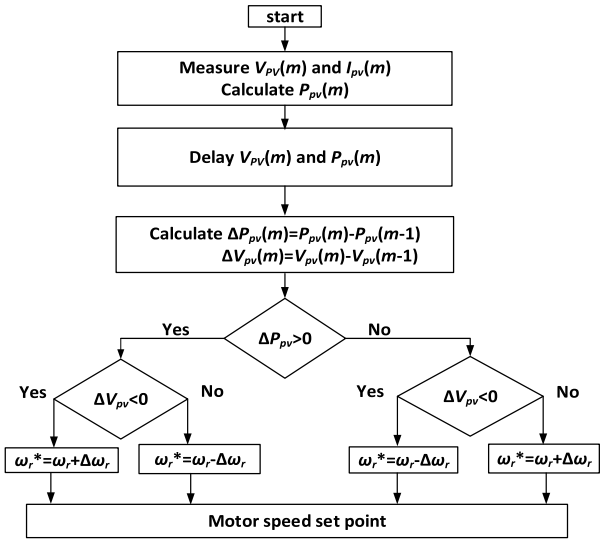

FIGURE 16. The MPPT strategy at time instant m.

about the DE optimizer applied to global MPP for PV system is presented in [42] and [41]. Implementation of mutation and crossover stages creates a trial vector ωu_{i} for each target vector. Then, a selection stage is carried out between trial and target vectors. The mechanism of the solution process for DE algorithm is explained as fellows; the motor speed is employed as a target vector and the solar PV output power represents the fitness function. Through the maximum and minimum speed limits $[\omega_{\min}, \omega_{\max}]$, the target vectors are randomly positioned. Then, the generated population of motor speeds is applied to PV pumping system. Then, the PV power is estimated via sensing PV current and voltage. After the initialization stage is completed, the largest PV power is nominated as P_{best} and the obtained motor speed ω_{i} is kept as the best choice ω_{best}. Then, two diverse population are arbitrarily chosen. A mutation factor F is employed to weight the difference among the chosen target vector. Next, the weighted difference is inserted into the best motor speed for generating donor vector ω_{vi}. The mutation stage that generates the donor vector (ωv_{i}) can be represented as fellows [38], [41]–[47].

$$\omega v_i = \omega_{best} + F \times (\omega_{r_1} - \omega_{r_2}) \tag{2}$$

where indexes r_1 and r_2 represent two different integers and F is ascale factor.

Then, the following equation can be used to check if the generated element is located in the specified range.

$$\omega v_i = \begin{cases} \omega v_i = \omega_{\max} \rightarrow & \text{if } \omega v_i \text{ greater than } \omega_{\max} \\ \omega v_i = \omega_{\min} \rightarrow & \textit{if } \omega v_i \text{ smaller than } \omega_{\min} \end{cases} \tag{3}$$

Then, the crossover stage is applied to create the trail vector ωu_{i} based on the following equation.

$$\omega u_i = \begin{cases} \omega v_i & \text{if } rand \leq C_r \\ \omega_i \end{cases} \tag{4}$$

C_r in (4) denotes the crossover control parameter.

TABLE 3. The description of different partial shading patterns.

Irradiation	Solar irradiance levels, W/m²	Power at GMPP	Voltage at GMPP	Current at GMPP
Uniform irradiance	1000	5621.0 W	743.82	7.6257
1st shadow pattern	1000 300	2836.1 W	371.91 V	7.6257 A
2nd shadow pattern	1000 800 400	3145.1 W	504.05 V	6.2396 A
3rd shadow pattern	1000 800 600 300	2812.0 W	603.4 V	4.6564 A

The final stage is the selection. It can be applied based on (5). The comparison among target and trial vectors is applied. Each trial vector is evaluated via PV pumping system and corresponding output power is estimated. Based on the comparison, the motor speed that matches the greatest value of the PV power is employed as the next target vector;

$$\omega_{i+1} = \begin{cases} \omega u_i & \text{if } f(\omega u_i) \geq f(\omega_i) \\ \omega_i & \text{otherwise.} \end{cases} \quad (5)$$

The optimization process continues until an ending criterion is met. The solution process of DE technique can be summarized by Fig. 17.

It is worth mention that the values of "Maximum Iterations" and "Population Size" are problem dependent and usually chosen by trial and error. The maximum iteration and population size are selected to be 10 and 5 respectively. The DE has only two main control parameters; the mutation scale factor and crossover control parameter. In our study, the mutation factor and crossover parameters of the DE are set to be 0.6 and 0.67 respectively based on [41].

IV. PERFORMANCE OF THE PROPOSED PV PUMPING SYSTEM

For evaluation and test the performance of the aforementioned system, extensive MATLAB simulation work is done. Here, we compare the performance of the system under two different MPPT algorithms i.e. P&O and DE. The system is studied under uniform irradiation and partial shadow conditions. In uniform irradiation case, the standard irradiance level (1000 W/m^2) is considered (see Fig. 12), while in partial shading case three different patterns for the irradiance is investigated as shown in Fig. 13. Under shadow condition, the bypass diodes which are parallel connected with each PV module will be forward biased and carry the generated current instead of shaded panel [49], [50]. On the other hand, these diodes have no influence under uniform distribution of solar irradiance since they are reversing biased. The studied PV pumping system comprises of 42 series-connected solar modules. Each module consists of 36 series-connected cells with a peak power of 135 Watt. The ideal output power of the PV system is 5.6 kWp (i.e. 42 × 135 W). To assess the influence of CPS, three various partial shadow patterns are used, as shown in Table 3. Figure 18 shows the power-voltage curves of PV system under uniform and partial shadow condition (three different patterns of CPS). It can be noticed that, the first, second and third patterns contain two, three and four peaks respectively, depending on the number of various levels of incident solar irradiance. The main idea of using the

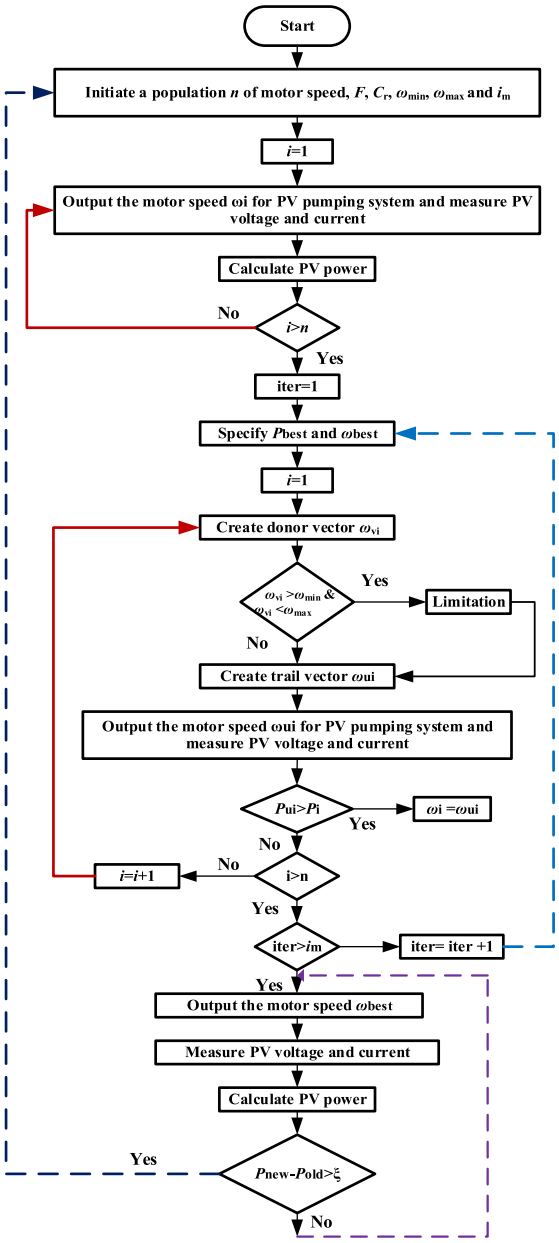

FIGURE 17. The solution process of DE technique.

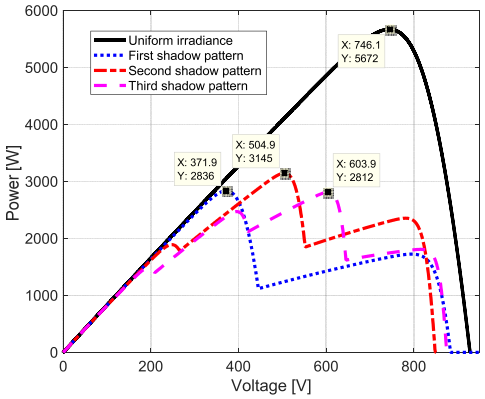

FIGURE 18. The power against voltage curves of solar array under uniform irradiance and three various patterns of CPS.

various patterns of CPS is to vary the position of the global MPP from left to middle to right to evaluate the performance of the DE-based tracker under different conditions as well as to assure the reliability of the DE-based tracker to extract the global MPP for any case of shadow effect.

A. UNIFORM IRRADIATION CASE

Under uniform irradiance case, one irradiance level, i.e. 1000 W/m^2, is used. Figures 19 to 21 show the performance of the system under a uniform irradiation level. Figure 19 shows the speed and torque response of the motor using the P&O and DE MPPT techniques. It is clear that the motor works at the rated speed (3000 rpm) and delivers the rated torque (17.38 N.m) successfully. Notice that, using P&O technique the motor speed increases until the PV output power is maximum, then it becomes constant. The time taken to catch the MPP using P&O is about 1.2 ms. However, using DE technique the motor starts with random speed and based on DE technique eventually, the optimum speed that maximizes the PV output power is obtained. The time taken to reach the MPP using DE technique is definitely much longer

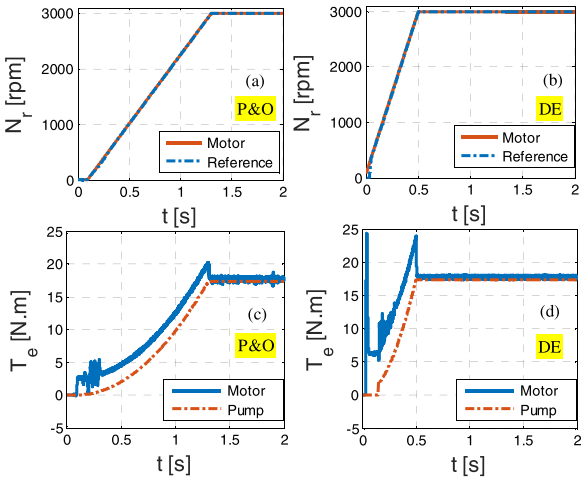

FIGURE 19. Run-up response of SynRM under uniform irradiation level.

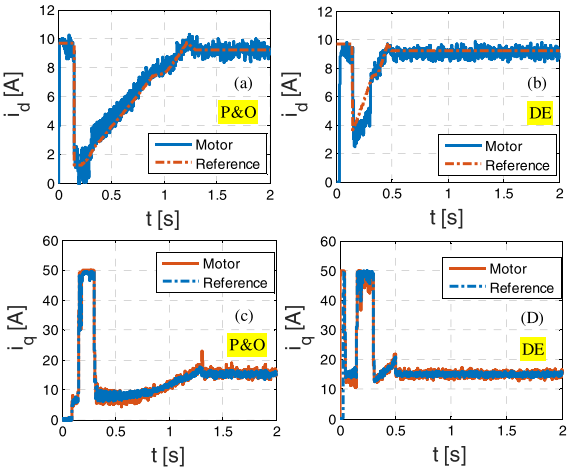

FIGURE 20. dq-axis current components of SynRM under uniform irradiation level.

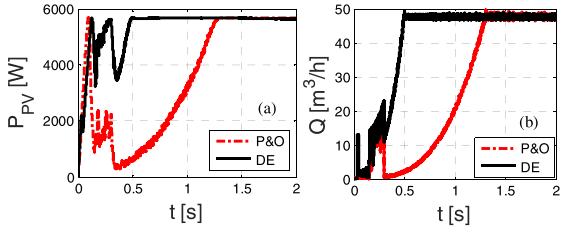

FIGURE 21. PV output power (a) and pump flow rate (b) under uniform irradiation level.

than the time taken using the P&O strategy under uniform irradiation levels over the PV modules. The presented results based on DE technique shown in Figs. 19 to 21 and in the rest of the paper are only of the final obtained speed that maximizes the PV output power. Figure 20 shows the *dq*axis currents of the motor using the two MPPT techniques. It is clear that the motor currents follow accurately the reference signals. In addition, the *dq* axis currents are similar using the conventional P&O and DE MPPT techniques. The PV array output power and the pump flow rate are shown in Fig. 21(a) and (b) respectively. Obvious, the PV array output power is maximum (see Fig. 18) based on both MPPT techniques.

Moreover, in this case, if the irradiation level is reduced, e.g. from 1000 W/m^2 to 750 W/m^2, the maximum available power of the PV array will be reduced as presented in Fig. 12, hence the output power of the motor will be reduced as shown in [33].

B. FIRST SHADOW PATTERN CASE

Figures 22 to 24 report the performance of the system under the first shadow pattern condition. Two different solar irradiation levels of 1000 and 300 W/m^2 are imposed to the PV array as a first shadow pattern. Under this case as illustrated in Fig. 18, the power against voltage curve has two peaks of MPPs. The global MPP of 2836 W exists at 371.91 V.

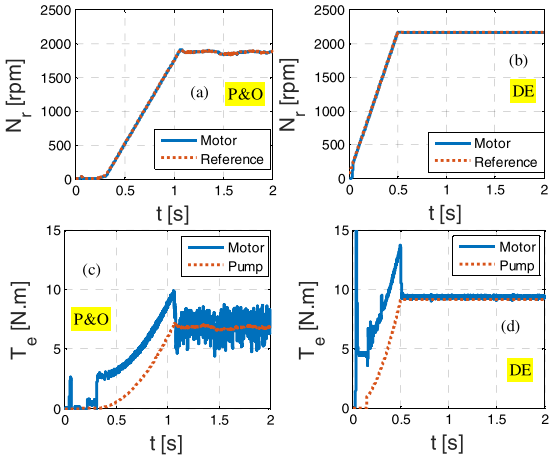

FIGURE 22. Run-up response of SynRM under shadow condition (First pattern).

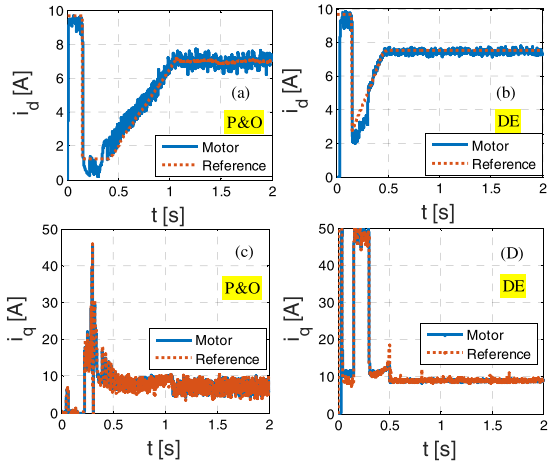

FIGURE 23. dq-axis current components of SynRM under shadow condition (First pattern).

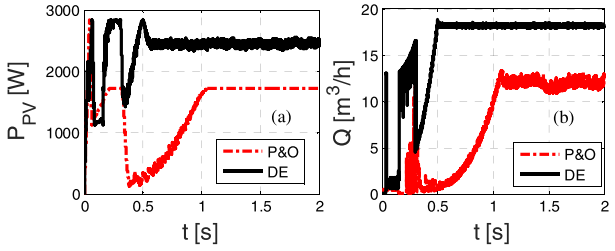

FIGURE 24. PV output power (a) and pump flow rate (b) under shadow condition (First pattern).

Figure 22 shows the speed and torque response of the motor under the first shadow pattern using the conventional P&O and DE MPPT techniques. Clearly, the motor speed using DE technique (Fig. 22(b) is much higher than the conventional P&O method (Fig. 22(a)) by about 14.81%. Consequently, the torque of the pump in case of using DE technique (Fig. 22 (d)) is higher than using P&O method (Fig. 22 (c)) because it is proportional to the motor speed. The dq-axis currents of the motor are shown in Fig. 23 using the two MPPT techniques. It is obvious that the motor currents follow accurately the reference signals. In addition, the dq-axis currents are different in the two MPPT techniques. This is because the torque of the motor is different. Figure 24(a) and (b) show the PV output power and the pump flow rate respectively. It is evident from Fig. 24(a) that the PV array can deliver much output power using the DE MPPT technique than P&O by about 41.90%. This also results in a high flow rate of the pump as shown in Fig. 24(b). The flow rate of the pump using DE MPPT technique is much higher than using P&O method by about 52%.

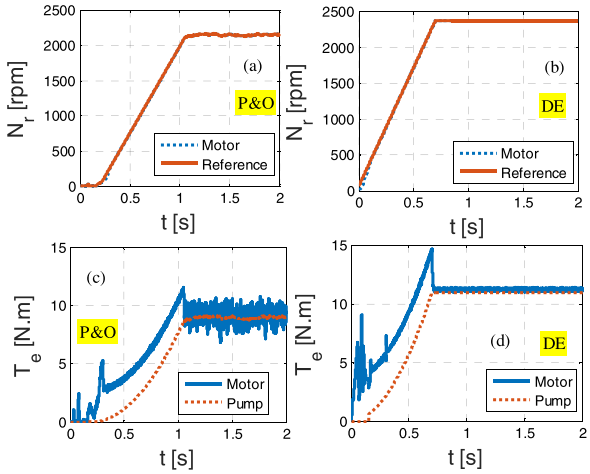

FIGURE 25. Run-up response of SynRM under shadow condition (Second pattern).

C. SECOND SHADOW PATTERN CASE

Figures 25 to 27 show the performance of the system under the second shadow pattern condition. Three different solar irradiance levels of 1000, 800 and 400 W/m^2 are imposed to the PV array as a second shadow pattern. In this case, the power versus the voltage curve of the PV array has three peaks of MPPs as displayed in Fig. 20. The global MPP of 3145.1 W exists at the center point of 504.05 V. Figure 25 shows the speed and torque response of the motor under the second shadow pattern using the conventional P&O and DE MPPT techniques. It is noticed that the motor speed using DE technique (Fig. 25(b) is higher than the conventional P&O method (Fig. 25(a)) by about 10.58%. Thereby, the torque of the pump in case of using DE technique (Fig. 25(d)) is higher than using P&O method (Fig. 25(c)) as explained before. The *dq*-axis currents of the motor are shown in Fig. 26 using the two MPPT techniques. It is clear that the motor currents follow accurately the reference signals. Figure 27(a) and (b) show the PV output power and the pump flow rate respectively. It is obvious from Fig. 27(a) that the PV array can give much output power using the DE MPPT technique than P&O by about 32.48%. This also results in a high flow rate of the pump as shown in Fig. 27(b). The flow rate of the pump using DE

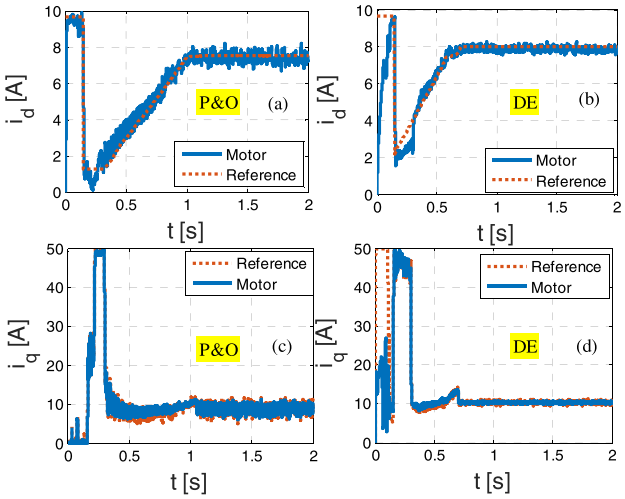

FIGURE 26. dq-axis current components of SynRM under shadow condition (Second pattern).

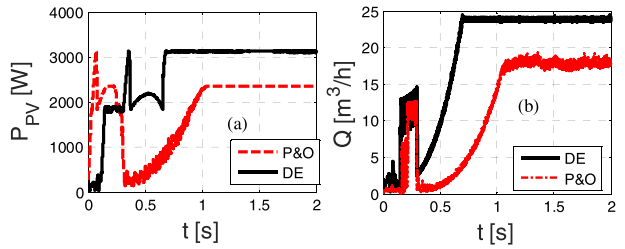

FIGURE 27. PV output power (a) and pump flow rate (b) under shadow condition (Second pattern).

MPPT technique is much higher than using P&O method by about 32.77%.

D. THIRD SHADOW PATTERN CASE

Figures 28 to 30 report the performance of the system under the third shadow pattern condition. Four different solar irradiance levels of 1000, 800, 600 and 300 W/m^2 are imposed to the PV array as a third shadow pattern. In this case, the power versus the voltage curve of the PV array has four peaks of MPPs as seen in Fig. 18. The global MPP of 2812 W exists at 603.4 V that is corresponding to the second right point on the power against voltage curve (see Fig. 18). Figure 28 displays the speed and torque response of the motor under the third shadow pattern using the conventional P&O and DE MPPT techniques. It is clear that the motor speed using DE technique (Fig. 28(b) is higher than the conventional P&O method (Fig. 28(a)) by about 17.88%. Therefore, the torque of the pump in case of using DE technique (Fig. 28(d)) is higher than using P&O method (Fig. 28(c)) as explained before. The *dq*-axis currents of the motor are shown in Fig. 29 using the two MPPT techniques. It is clear that the motor currents follow accurately the reference signals.

Figure 30(a) and (b) show the PV output power and the pump flow rate respectively. It is obvious from Fig. 30(a) that the PV array can give much output power using the DE MPPT

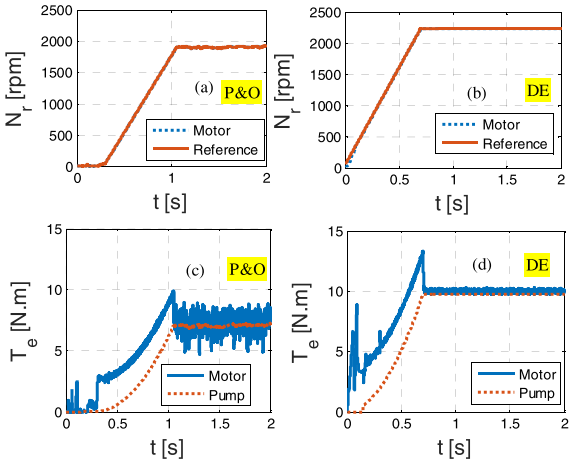

FIGURE 28. Run-up response of SynRM under shadow condition (Third pattern).

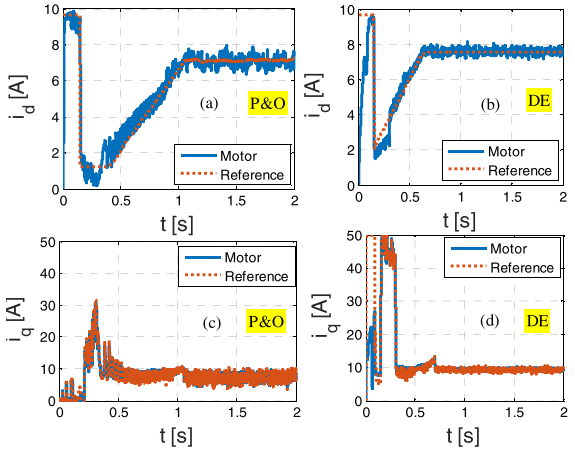

FIGURE 29. dq-axis current components of SynRM under shadow condition (Third pattern).

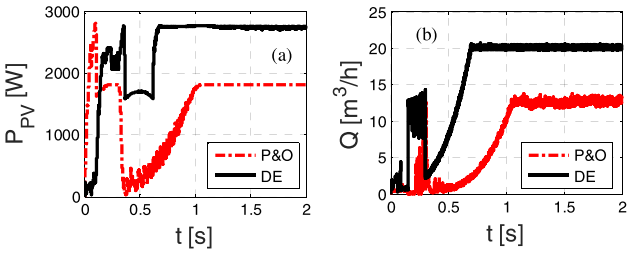

FIGURE 30. PV output power (a) and pump flow rate (b) under shadow condition (Third pattern).

technique than P&O by about 50.48%. This also results in a high flow rate of the pump as shown in Fig. 30(b). The flow rate of the pump using DE MPPT technique is much higher than using P&O method by about 61.60%.

The updating process of the motor speed during searching process of DE MPPT technique for the aforementioned cases are shown in Fig. 31. Notice that, each color in Fig. 31 represents one particle (motor speed) of the population size (five particles).

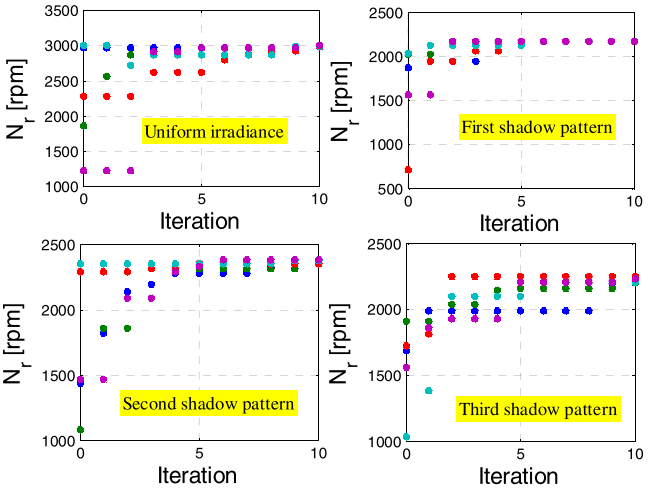

FIGURE 31. The updating process of the motor speed during searching process of DE-based tracker.

It is observed in the previous figures that higher transients in case of DE compared to P&O are seen. This is because the variation rate of the speed set point from 0 to the steady-state value is much higher in case of DE. This results in higher transients in the current and hence the torque.

V. EXPERIMENTAL VALIDATION

To validate the theoretical work shown in this paper, the experimental setup in Fig. 32 is constructed. A 5.5 kW prototype SynRM is connected via a torque sensor with a 9.3 kW induction motor. A conventional inverter (VSI) is utilized to drive the SynRM. The control system shown before in Figs. 15 and 16 is implemented in DS1103 platform and is employed to drive the SynRM. An incremental encoder of 1024 sample/revolution is employed to measure the speed of the motor. Three current sensors (LA25-P) are used to measure the SynRM currents. The electrical components of the system such as voltage, current, power factor are measured by a power analyzer. A DC controlled supply is emulated the PV array; the maximum allowed voltage and current of the DC supply are 605 V and 17 A respectively. The induction motor is driven by a commercial inverter in the torque control model in order to emulate the various loading conditions of the pump.

The four studied cases before, i.e. uniform irradiance, first shadow pattern, second shadow pattern and third shadow pattern, are implemented experimentally on the test bench shown in Fig. 23. The simulated results using P&O and DE MPPT schemes are shown in Table 4 for the different cases. In the Table 4, the I_{Ph}, N_r, P_o and V_{dc} stand for the phase current, speed, output power of the SynRM and the DC bus voltage of the inverter respectively. To validate the simulated results, the DC bus voltage of the inverter and the reference speed of the SynRM control are given based on the obtained simulated values using P&O and DE MPPT schemes (Tables). Notice that, the maximum permitted DC voltage in the experiments

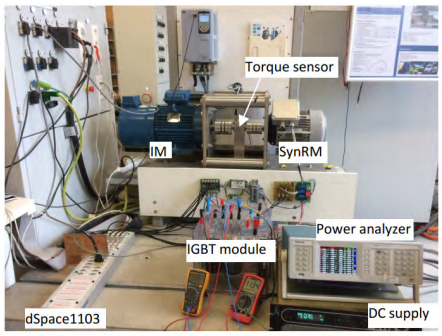

FIGURE 32. A photograph of the experimental setup.

TABLE 4. Comparison between simulated and measured results of different cases.

Uniform irradiance	Simulations		Measurements	
Variable	**P&O**	**DE**	**P&O**	**DE**
I_{ph} (A)	12.23	12.23	12.23	12.23
N_r(rpm)	3000	3000	3000	3000
P_o(W)	5435	5435	5272	5272
V_{dc} (V)	755	755	605	605
First shadow	**Simulations**		**Measurements**	
Variable	**P&O**	**DE**	**P&O**	**DE**
I_{ph} (A)	7	8.25	7	8.25
N_r(rpm)	1875	2172	1875	2172
P_o(W)	1325.35	1535.30	1286	1486
V_{dc} (V)	793.2	410	605	410
Second shadow	**Simulations**		**Measurements**	
Variable	**P&O**	**DE**	**P&O**	**DE**
I_{ph} (A)	8.28	9.15	8.28	9.15
N_r(rpm)	2156.5	2381	2156.5	2381
P_o(W)	2021.16	2231.36	1951	2160
V_{dc} (V)	782	510	605	510
Third shadow	**Simulations**		**Measurements**	
Variable	**P&O**	**DE**	**P&O**	**DE**
I_{ph} (A)	7.07	8.42	7.07	8.42
N_r(rpm)	1917.5	2248	1917.5	2248
P_o(W)	1618.44	1897.4	1569	1836
V_{dc} (V)	815	605	605	605

(605 V) is used for all simulated points having a DC voltage higher than 605 V. Further, the induction motor, that emulates the pump, is controlled to provide the load torque that makes the SynRM absorbing the phase current listed in Table 4. Thus, the output power of the motor is measured for each case, see Table 4. A good matching between the measurements and simulations is evident. The measured results validate the operating conditions of both P&O and DE MPPT schemes.

To better understand the results in Table 4, as an example, the result of uniform irradiance case using P&O method is shown here. The load torque produced the induction motor

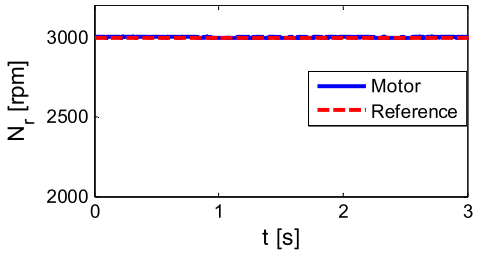

FIGURE 33. Measured SynRM speed versus the time.

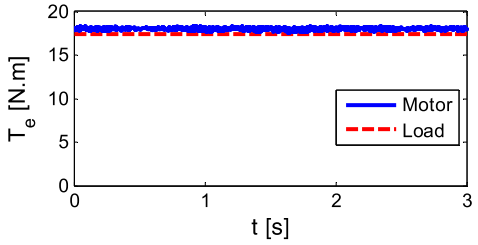

FIGURE 34. Measured torque versus the time.

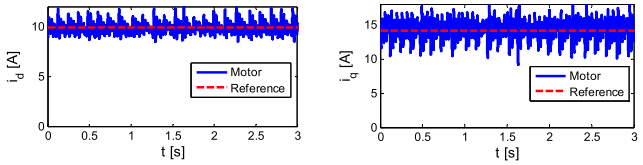

FIGURE 35. Measured dq- axis currents versus the time.

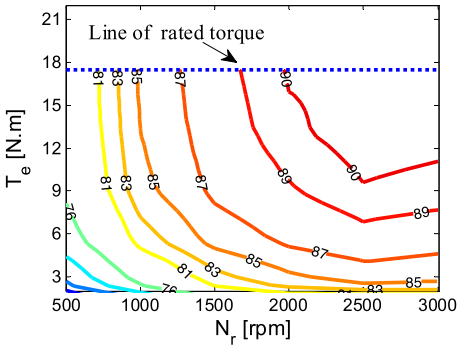

FIGURE 36. Measured efficiency map of the whole drive using SynRM.

is set at the rated value of the pump and the rated speed (3000 rpm) is given as a set point for the SynRM control of Fig. 15. The current set point i_d* in Fig. 15 is obtained from a lookup table (from FEM) based on the load torque to fulfill the maximum torque per Ampère condition for the SynRM. Figure 33 shows the measured speed of the reference and the motor at a steady state operation. The motor speed follows accurately the set point. Figure 34 shows the measured torque of the given load and the motor as a function of time. The motor can provide the required load torque. The measured dq-axis currents are shown in Fig. 35. The measured efficiency map of the whole drive (prototype+ inverter) is reported in Fig. 36. For different load torque, the d-axis current is obtained to achieve the maximum torque per Ampère condition. It is clear that the efficiency of SynRM is good even for low load torque and speed. Consequently, the whole solar system efficiency will be improved.

VI. CONCLUSIONS

In this paper, an improved performance of a solar photovoltaic system employing synchronous reluctance motor (SynRM) for pumping application is shown. The system does not use the DC-DC converter for maximizing the output power of the PV array. In addition, storage batteries are not included as well. The conventional voltage source inverter is employed to drive the system in an efficient way using a proposed control system. The performance of the proposed system under two different MPPT methods i.e. perturbation and observation (P&O) and differential Evolution (DE) techniques is studied under uniform and partial shadow irradiation conditions. Three different partial shading patterns are investigated.

It is found that under the first shadow pattern, the motor speed using DE technique is higher than the conventional P&O one by about 14.81 %. Consequently, the PV array delivers much output power using the DE than P&O by about 41.90%. This results in a higher flow rate of the pump by about 52%. Under the second shadow pattern, the motor speed using DE technique is higher than the conventional P&O method by about 10.58 %. Hence, the PV array gives much output power using the DE by about 32.48%. Accordingly, the flow rate of the pump is increased by about 32.77%. Under the third shadow pattern, the motor speed is increased by about 17.88%. Therefore, the PV array supplies much output power using the DE compared to P&O by about 50.48%. Thus, the flow rate of the pump increased by about 61.60%. However under uniform irradiation level, both MPPT techniques can enable the PV array to provide the available maximum power. In general, it can be concluded that the MPPT based on DE method improves the PV pumping system performance compared to P&O method under the partial shadow condition. Experimental measurements are obtained to validate the theoretical work presented in this paper.

APPENDIX

MODELLING OF THE PROPOSED PV PUMPING SYSTEM

In this section, the mathematical model of the different components employed in the proposed system is given:

1) PV ARRAY MODEL

The solar cell model of a one diode sketched in Fig. A11 is used. The practical PV module includes several series-connected solar cells.

The solar cell output current can be represented as fellows [2], [3]:

$$I_{PV} = I_{ph} - I_o \left[\exp\left(\frac{V_{PV} + R_s I_{PV}}{V_t a} \right) - 1 \right] - \frac{V_{PV} + R_{sm} I_{PV}}{R_{pm}} \quad \text{(A11)}$$

where I_{pv} and V_{pv} are the current and voltage of the solar module; I_o and I_{ph} are the saturation and photocurrents; V_t is the thermal voltage of the module; a is the diode ideality factor; R_{sm} and R_{pm} are the series and parallel resistance of the module.

The photocurrent depends mostly on the solar irradiance intensity and cell temperature. It can be formulated as fellows [4]:

$$I_{ph} = \left(I_{sc} + k_i \left(T_c - T_{ref}\right)\right) G \tag{A12}$$

where I_{sc} is the module short-circuit current at standard conditions (25°C and 1000 W/m^2); k_i is the temperature coefficient of the short-circuit current (A/°C); T_{ref} is the cell reference temperature; G is the solar irradiation level (W/m^2).

Moreover, the following relation can be used to estimate the diode saturation current [4]:

$$I_o = I_{rs} \left(\frac{T_c}{T_{ref}}\right)^3 \exp\left(\frac{qE_G}{kA}\left(\frac{1}{T_{ref}} - \frac{1}{T_c}\right)\right) \tag{A13}$$

where I_{rs} is the cell reverse saturation current at the reference temperature and the solar irradiation and E_G is the bang-gap energy of the semiconductor used in the cell.

The PV array is a series and parallel connection of the modules. Hence for a given number of series (N_s) and parallel (N_p) modules, the equivalent *I-V* relation can be as follows [4]:

$$I_{PV} = I_{ph}N_p - I_oN_p \left[\exp\left(\frac{V_{PV} + R_{sm}I_{PV}\left(\frac{N_s}{N_p}\right)}{V_t a N_s}\right) - 1\right] - \frac{V_{PV} + R_{sm}I_{PV}\left(\frac{N_s}{N_p}\right)}{R_{pm}\left(\frac{N_s}{N_p}\right)} \tag{A14}$$

2) THREE PHASE INVERTER MODEL

The output voltage of the inverter can be represented in terms of PV array voltage as follows [3]; with K_1, K_2 and K_3 the switching states of the 3 inverter legs, being either 1 or 0. When the switch state (K_1, K_2 or K_3) equals 1, it means that the corresponding upper switch is ON while the lower one is OFF and vice versa. The IGBTs of the inverter are assumed to be ideal which means that the conduction losses of the inverter are not taken into account.

$$\begin{aligned} v_{an} &= \frac{1}{3}(2K_1 - K_2 - K_3)V_{dc} \\ v_{bn} &= \frac{1}{3}(-K_1 + 2K_2 - K_3)V_{dc} \\ v_{cn} &= \frac{1}{3}(-K_1 - K_2 + 2K_3)V_{dc} \end{aligned} \tag{A15}$$

3) SYNRM MODEL

The SynRM is modelled in *dq*-axis rotor reference frame. The detailed model given in [18] is used in this study. The main SynRM model equations are as follows [18]:

$$\left.\begin{aligned} v_d &= R_s i_d + p\lambda_d(i_d, i_q) - \omega_r P\lambda_q(i_d, i_q) \\ v_q &= R_s i_q + p\lambda_q(i_d, i_q) + \omega_r P\lambda_d(i_d, i_q) \\ T_e &= \frac{3}{2}P(\lambda_d(i_d, i_q)i_q - \lambda_q(i_d, i_q)i_d) \end{aligned}\right\} \tag{A16}$$

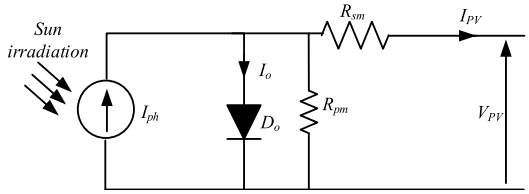

FIGURE 37. One diode solar cell equivalent circuit.

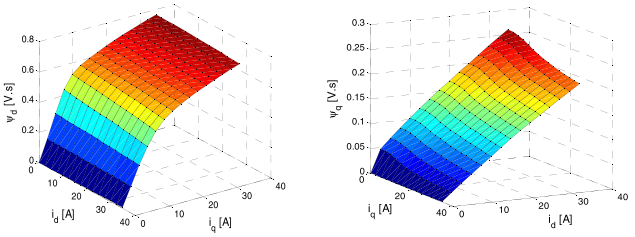

FIGURE 38. Direct (d) and quadrature (q) axis flux-linkages of the SynRM versus the current components.

where (v_d, v_q), (i_d, i_q) and (λ_d, λ_q) indicate the voltage, current and flux linkage of the direct and quadrature axis components of the motor respectively; R_s and T_e denote the winding resistance and the electromagnetic torque; P and p are the pole pairs number and the differential operator; ω_r is the rotor mechanical speed.

It is clear from (A16) that the SynRM performance depends mainly on the *dq*-axis flux-linkages which in turn to be the magnetic saturation behavior of the machine; this is explained very well in [18]. Consequently, a model to include the magnetic saturation behavior of the machine is necessary. Here, the magnetic saturation of *dq*-axis flux-linkages of the machine is considered as shown in Fig. 38 using lookup tables (LUTs). These LUTs are generated from FEM. In FEM, both i_d and i_q are varied within a range up to double rated current to obtain the corresponding behavior of the *dq* axis flux-linkages (ψ_d, ψ_q). This way is efficient in including the correct behavior of the magnetic saturation in the SynRM modelling.

4) CENTRIFUGAL PUMP MODEL

The torque (T_{cp})-speed (ω_r) relation of the centrifugal pump is represented by [6]–[8]:

$$T_{cp} = K_p\omega_r^2 \tag{A17}$$

where K_p is the proportionality constant of the pump and ω_r is the rotational speed of the rotor in rad/s. The K_p value is calculated based on the rated torque and speed offered by the motor.

REFERENCES

[1] S. S. Chandel, M. N. Naik, and R. Chandel, "Review of solar photovoltaic water pumping system technology for irrigation and community drinking water supplies," *Renew. Sustain. Energy Rev.*, vol. 49, pp. 1084–1099, Sep. 2015.

[2] V. C. Sontake and V. R. Kalamkar, "Solar photovoltaic water pumping system—A comprehensive review," *Renew. Sustain. Energy Rev.*, vol. 59, pp. 1038–1067, Jun. 2016.
[3] M. Nabil, S. M. Allam, and E. M. Rashad, "Modeling and design considerations of a photovoltaic energy source feeding a synchronous reluctance motor suitable for pumping systems," *Ain Shams Eng. J.*, vol. 3, no. 4, pp. 375–382, Dec. 2012.
[4] M. Nabil, S. M. Allam, and E. M. Rashad, "Performance improvement of a photovoltaic pumping system using a synchronous reluctance motor," *Electr. Power Compon. Syst.*, vol. 41, no. 4, pp. 447–464, Feb. 2013.
[5] E. Mahmoud and H. el Nather, "Renewable energy and sustainable developments in Egypt: Photovoltaic water pumping in remote areas," *Appl. Energy*, vol. 74, nos. 1–2, pp. 141–147, Jan. 2003.
[6] A. A. Hamza and A. Z. Taha, "Performance of submersible PV solar pumping systems under conditions in the Sudan," *Renew. Energy*, vol. 6, nos. 5–6, pp. 491–495, Jul./Sep. 1995.
[7] A. Hamidat, B. Benyoucef, and T. Hartani, "Small-scale irrigation with photovoltaic water pumping system in Sahara regions," *Renew. Energy*, vol. 28, no. 7, pp. 1081–1096, Jun. 2003.
[8] A. Chaurey, P. M. Sadaphal, and D. Tyaqi, "Experiences with SPV water pumping systems for rural applications in India," *Renew. Energy*, vol. 3, no. 8, pp. 961–964, Nov. 1993.
[9] A. S. A. Nafeh, "Design and economic analysis of a stand-alone PV system to electrify a remote area household in Egypt," *Open Renew. Energy J.*, vol. 2, no. 1, pp. 33–37, Apr. 2009.
[10] E. R. Shouman, E. T. El Shenawy, and M. A. Badr, "Economics analysis of diesel and solar water pumping with case study water pumping for irrigation in Egypt," *Int. J. Appl. Eng. Res.*, vol. 11, no. 2, pp. 950–954, 2016.
[11] S. M. Alghuwainem, "Matching of a DC motor to a photovoltaic generator using a step-up converter with a current-locked loop," *IEEE Trans. Energy Convers.*, vol. 9, no. 1, pp. 192–198, Mar. 1994.
[12] R. Kumar and B. Singh, "BLDC motor driven solar PV array fed water pumping system employing zeta converter," in *Proc. IEEE 6th India Int. Conf. Power Electron. (IICPE)*, Dec. 2014, pp. 1–6.
[13] R. Kumar and B. Singh, "BLDC motor-driven solar PV array-fed water pumping system employing zeta converter," *IEEE Trans. Ind. Appl.*, vol. 52, no. 3, pp. 2315–2322, May 2016.
[14] R. Antonello, M. Carraro, Al. Costabeber, F. Tinazzi, and M. Zigliotto, "Energy-efficient autonomous solar water-pumping system for permanent-magnet synchronous motors," *IEEE Trans. Ind. Electron.*, vol. 64, no. 1, pp. 43–51, Jan. 2017.
[15] B. Singh, A. K. Mishra, and R. Kumar, "Solar powered water pumping system employing switched reluctance motor drive," *IEEE Trans. Ind. Appl.*, vol. 52, no. 5, pp. 3949–3957, Sep./Oct. 2016.
[16] B. Singh and R. Kumar, "Solar photovoltaic array fed water pump driven by brushless DC motor using Landsman converter," *IET Renew. Power Gener.*, vol. 10, no. 4, pp. 474–484, Apr. 2016.
[17] Z. Yang, F. Shang, I. P. Brown, and M. Krishnamurthy, "Comparative study of interior permanent magnet, induction, and switched reluctance motor drives for EV and HEV applications," *IEEE Trans. Transport. Electrific.*, vol. 1, no. 3, pp. 245–254, Oct. 2015.
[18] M. N. Ibrahim, P. Sergeant, and E. M. Rashad, "Relevance of including saturation and position dependence in the inductances for accurate dynamic modeling and control of SynRMs," *IEEE Trans. Ind. Appl.*, vol. 53, no. 1, pp. 151–160, Jan./Feb. 2017.
[19] J. Appelbaum, "Starting and steady-state characteristics of DC motors powered by solar cell generators," *IEEE Trans. Energy Convers.*, vol. EC-1, no. 1, pp. 17–25, Mar. 1986.
[20] H. M. B. Metwally and W. R. Anis, "Dynamic performance of directly coupled photovoltaic water pumping system using D.C. shunt motor," *Energy Convers. Manage.*, vol. 37, no. 9, pp. 1407–1416, Sep. 1996.
[21] Z. Zinger and A. Braunstein, "Optimum operation of a combined system of a solar cell array and a DC motor," *IEEE Trans. Power App. Syst.*, vol. PAS-100, no. 3, pp. 1193–1197, Mar. 1981.
[22] M. M. Saied, "Matching of DC motors to photovoltaic generators for maximum daily gross mechanical energy," *IEEE Trans. Energy Convers.*, vol. 3, no. 3, pp. 465–472, Sep. 1988.
[23] W. Z. Fam and M. K. Balachander, "Dynamic performance of a DC shunt motor connected to a photovoltaic array," *IEEE Trans. Energy Convers.*, vol. 3, no. 3, pp. 613–617, Sep. 1988.
[24] V. C. Mummadi, "Steady-state and dynamic performance analysis of PV supplied DC motors fed from intermediate power converter," *Sol. Energy Mater. Sol. Cells*, vol. 61, no. 4, pp. 365–381, Apr. 2000.
[25] Y. R. Hsiao and B. A. Blevins, "Direct coupling of photovoltaic power source to water pumping system," *Sol. Energy*, vol. 32, no. 4, pp. 489–498, 1984.
[26] S. Singer and J. Appelbaum, "Starting characteristics of direct current motors powered by solar cells," *IEEE Trans. Energy Convers.*, vol. 8, no. 1, pp. 47–53, Mar. 1993.
[27] A. Betka and A. Moussi, "Performance optimization of a photovoltaic induction motor pumping system," *Renew. Energy*, vol. 29, no. 14, pp. 2167–2181, Nov. 2004.
[28] R. Kumar and B. Singh, "Single stage solar PV fed brushless DC motor driven water pump," *IEEE J. Emerg. Sel. Topics Power Electron.*, vol. 1, no. 3, pp. 1377–1385, Sep. 2017.
[29] P. Packiam, N. K. Jain, and I. P. Singh, "Steady and transient characteristics of a single stage PV water pumping system," *Energy Syst.*, vol. 6, no. 2, pp. 173–199, Jun. 2015.
[30] A. B. Raju, S. R. Kanik, and R. Jyoti, "Maximum efficiency operation of a single stage inverter fed induction motor PV water pumping system," in *Proc. 1st Int. Conf. Emerg. Trends Eng. Technol.*, Jul. 2008, pp. 905–910.
[31] A. T. De Almeida, F. J. T. E. Ferreira, and A. Q. Duarte, "Technical and economical considerations on super high-efficiency three-phase motors," *IEEE Trans. Ind. Appl.*, vol. 50, no. 2, pp. 1274–1285, Mar./Apr. 2014.
[32] A. Varshney and B. Singh, "Performance of SPV array fed pumping system with synchronous reluctance motor drive," in *Proc. IEEE 1st Int. Conf. Power Electron., Intell. Control Energy Syst. (ICPEICES)*, Jul. 2016, pp. 1–6.
[33] M. N. Ibrahim, P. Sergeant, and E. M. Rashad, "Design of low cost and efficient photovoltaic pumping system utilizing synchronous reluctance motor," in *Proc. IEEE Int. Electr. Mach. Drives Conf. (IEMDC)*, Miami, FL, USA, May 2017, pp. 1–7.
[34] K. Benlarbi, L. Mokrani, and M. S. Nait-Said, "A fuzzy global efficiency optimization of a photovoltaic water pumping system," *Sol. Energy*, vol. 77, no. 2, pp. 203–216, 2004.
[35] M. G. Villalva, J. R. Gazoli, and E. R. Filho, "Comprehensive approach to modeling and simulation of photovoltaic arrays," *IEEE Trans. Power Electron.*, vol. 24, no. 5, pp. 1198–1208, May 2009.
[36] H. Rezk and A. M. Eltamaly, "A comprehensive comparison of different MPPT techniques for photovoltaic systems," *Solar Energy*, vol. 112, pp. 1–11, Feb. 2015.
[37] J. Ahmed and Z. Salam, "A maximum power point tracking (MPPT) for PV system using cuckoo search with partial shading capability," *Appl. Energy*, vol. 119, pp. 118–130, Apr. 2014.
[38] Y.-H. Liu, S.-C. Huang, J.-W. Huang, and W.-C. Liang, "A particle swarm optimization-based maximum power point tracking algorithm for PV systems operating under partially shaded conditions," *IEEE Trans. Energy Convers.*, vol. 27, no. 4, pp. 1027–1035, Dec. 2012.
[39] M. Sarvi, S. Ahmadi, and S. Abdi, "A PSO-based maximum power point tracking for photovoltaic systems under environmental and partially shaded conditions," *Prog. Photovolt., Res. Appl.*, vol. 23, no. 2, pp. 201–214, 2015.
[40] J. Ma, K. L. Man, T. O. Ting, N. Zhang, C.-U. Lei, and N. Wong, "Low-cost global MPPT scheme for photovoltaic systems under partially shaded conditions," in *Proc. IEEE Int. Symp. Circuits Syst. (ISCAS)*, May 2013, pp. 245–248.
[41] K. S. Tey, S. Mekhilef, H.-T. Yang, and M.-K. Chuang, "A differential evolution based MPPT method for photovoltaic modules under partial shading conditions," *Int. J. Photoenergy*, vol. 2014, pp. 1–10, May 2014.
[42] A. A. Z. Diab and H. Rezk, "Global MPPT based on flower pollination and differential evolution algorithms to mitigate partial shading in building integrated PV system," *Solar Energy*, vol. 157, pp. 171–186, Nov. 2017.
[43] R. Sridhar, S. Jeevananthan, S. S. Dash, and P. Vishnuram, "A new maximum power tracking in PV system during partially shaded conditions based on shuffled frog leap algorithm," *J. Exp. Theor. Artif. Intell.*, vol. 29, no. 3, pp. 481–493, 2016.
[44] L. L. Jiang, D. L. Maskell, and J. C. Patra, "A novel ant colony optimization-based maximum power point tracking for photovoltaic systems under partially shaded conditions," *Energy Buildings*, vol. 58, no. 1, pp. 227–236, Mar. 2013.
[45] K. Chen, S. Tian, Y. Cheng, and L. Bai, "An improved MPPT controller for photovoltaic system under partial shading condition," *IEEE Trans. Sustain. Energy*, vol. 5, no. 3, pp. 978–985, Jul. 2014.
[46] S. M. Mirhassani, S. Z. M. Golroodbari, S. M. M. Golroodbari, and S. Mekhilef, "An improved particle swarm optimization based maximum power point tracking strategy with variable sampling time," *Int. J. Elect. Power Energy Syst.*, vol. 64, pp. 761–770, Jan. 2015.

[47] K. Ishaque and Z. Salam, "A deterministic particle swarm optimization maximum power point tracker for photovoltaic system under partial shading condition," *IEEE Trans. Ind. Electron.*, vol. 60, no. 8, pp. 3195–3206, Aug. 2013.
[48] H. Rezk, A. Fathy, and A. Y. Abdelaziz, "A comparison of different global MPPT techniques based on meta-heuristic algorithms for photovoltaic system subjected to partial shading conditions," *Renew. Sustain. Energy Rev.*, vol. 74, pp. 377–386, Jul. 2017.
[49] H. Rezk and A. Fathy, "Simulation of global MPPT based on teaching–learning-based optimization technique for partially shaded PV system," *Elect. Eng.*, vol. 99, no. 3, pp. 847–859, 2017.
[50] A. Fathy and H. Rezk, "A novel methodology for simulating maximum power point trackers using mine blast optimization and teaching learning based optimization algorithms for partially shaded photovoltaic system," *J. Renew. Sustain. Energy*, vol. 8, no. 2, 2016, Art. no. 023503.
[51] N. Kumar, I. Hussain, B. Singh, B. K. Panigrahi, "Rapid MPPT for uniformly and partial shaded PV system by using JayaDE algorithm in highly fluctuating atmospheric conditions," *IEEE Trans. Ind. Informat.*, vol. 13, no. 5, pp. 2406–2416, Oct. 2017.
[52] X. Liu, F. Li, and Z. Na, "Optimal resource allocation in simultaneous cooperative spectrum sensing and energy harvesting for multichannel cognitive radio," *IEEE Access*, vol. 5, pp. 3801–3812, 2017.
[53] X. Liu, M. Jia, Z. Na, W. Lu, and F. Li, "Multi-modal cooperative spectrum sensing based on dempster-shafer fusion in 5G-based cognitive radio," *IEEE Access*, vol. 6, pp. 199–208, 2018.

MOHAMED N. IBRAHIM received the B.Sc. degree in electrical power and machines engineering from Kafrelshiekh University, Egypt, in 2008, the M.Sc. degree in electrical power and machines engineering from Tanta University, Egypt, in 2012, and the Ph.D. degree in Electromechanical Engineering from Ghent University, Belgium, in 2017. In 2008, he became a Teaching Assistant with the Electrical Engineering Department, Kafrelshiekh University. He was an Assistant Professor (on leave) with the Department of Electrical Engineering, Kafrelshiekh University. He is currently a Postdoctoral Researcher with the Department of Electrical Energy, Metals, Mechanical Constructions and Systems, Ghent University, Belgium. His current research interest includes design and control of electrical machines and drives for industrial and sustainable energy applications. He received several times the Kafrelshiekh University Award for his international scientific publications.

HEGAZY REZK received the B.Eng. and M.Eng. degrees in electrical engineering from Minia University, Egypt, in 2001 and 2006, respectively, and the Ph.D. degree from the Moscow Power Engineering Institute, Moscow. He was an Associate Professor (on leave) with the Electrical Engineering Department, Minia University. He was a Postdoctoral Research Fellow with the Moscow State University of Mechanical Engineering, Russia, for 6 months. He was a Visiting Researcher with Kyushu University, Japan. He is currently an Associate Professor with the Electrical Engineering Department, Collage of Engineering at Wadi Addwaser, Prince Sattam University, Saudi Arabia. He authored more than 50 technical papers. His current research interests include renewable energy, smart grid, hybrid systems, power electronics, and optimization and artificial intelligence.

MUJAHED AL-DHAIFALLAH received the B.Sc. and M.Sc. degrees in systems engineering from the King Fahd University of Petroleum and Minerals, Dhahran, Saudi Arabia, and the Ph.D. degree in electrical and computer engineering from the University of Calgary, Calgary, AB, Canada. He has been an Assistant Professor of systems engineering with the King Fahd University of Petroleum and Minerals, since 2009. His current research interests include nonlinear systems identification, control systems, optimization, artificial intelligence, and renewable energy.

PETER SERGEANT received the M.Sc. degree in electromechanical engineering and the Ph.D. degree in engineering sciences from Ghent University, Ghent, Belgium, in 2001 and 2006, respectively. In 2001, he became a Researcher with the Electrical Energy Laboratory, Ghent University. He became a Postdoctoral Researcher with Ghent University, in 2006, (Postdoctoral Fellow of the Research Foundation, Flanders), where he has been an Associate Professor, since 2012. He is currently a Professor of electrical drives with Ghent University and also a Core Lab Manager with Cluster Motion Products, Flanders Make. His current research interests include electrical machines and drives for industrial and for sustainable energy applications, with a focus on accurate computation of losses in machines and drives, improving energy efficiency, and increasing power density.